HHS Public Access

Author manuscript

Neurobiol Aging. Author manuscript; available in PMC 2018 January 01.

Published in final edited form as:

Neurobiol Aging. 2017 January ; 49: 198–203. doi:10.1016/j.neurobiolaging.2016.09.009.

Genetically Heterogeneous Mice Show Age-related Vision Deficits Not Related to Increased Rod Cell L-type Calcium Channel Function *In Vivo*

Bruce A. Berkowitz[1,2], **Richard A. Miller**[3], and **Robin Roberts**[2]

[1]Dept. of Anatomy and Cell Biology, Wayne State University School of Medicine, Detroit, MI

[2]Dept. Of Ophthalmology, Wayne State University School of Medicine, Detroit, MI

[3]Dept. Of Pathology, University of Michigan, Ann Arbor, MI

Abstract

Visual performance declines over time in humans and 2-18 mo outbred Long-Evans (LE) rats; vision is maintained in inbred 2- 18 mo C57BL/6 (B6) mice. Increased rod L-type calcium channel (LTCC) function predicts visual decline in LE rats but does not occur in B6 mice. Genetic diversity may contribute to rod LTCC function escalation time. To test this hypothesis, 4 and 18 mo genetically heterogeneous UM-HET3 mice were studied. Rod LTCC function (manganese-enhanced MRI), and ocular anatomy (MRI, optical coherence tomography, were measured *in vivo*. Light-evoked subretinal space (SRS) and choroid thickness changes were measured (diffusion-weighted MRI). Visual performance declined over time in the absence of i) increased rod LTCC function, ii) changes in light-dependent expansion of the SRS and choroidal thickness, and iii) retinal thinning. Aging changed anterior and vitreous chambers axial length, and decreased light-stimulated choroidal expansion. Species differences appear to contribute to the LTCC function differences. Aging-related declines in vision in the UM-HET3 mice deserve more attention than they have received so far.

Keywords

MEMRI; OKT; retina; aging

Introduction

Age-related physiologic vision loss - in which visual performance declines with aging in the absence of disease - remains largely untreatable, and aging is also a major risk factor in many disease-related visual problems. While the extent of vision loss with age in healthy patients is modest, its occurrence alone is a significant predictor of degrading day-to-day

Corresponding author: Bruce A. Berkowitz, Ph.D., Department of Anatomy and Cell Biology, Wayne State University School of Medicine, 540 E. Canfield, Detroit, MI 48201, (313) 577-9035, baberko@med.wayne.edu.

quality of life, deleterious aging outcomes (e.g., hip fracture), and reduced survival (Swindell et al., 2010). The rapid growth of the aging population raises an urgent and continuing need to understand the origins of age-related physiologic and disease-related vision loss (Bissig et al., 2013). Improved knowledge of the functional physiology of the "healthy" aging retina is essential to develop drug treatments with the goal of slowing normal retinal aging and delaying the onset of age-related physiologic and perhaps disease-related loss of vision.

L-type calcium channel can be non-invasively measured by manganese-enhanced MRI (MEMRI). This method takes advantage of the fact that retinal uptake *in vivo* of the strong MRI contrast agent and calcium ion surrogate manganese (Mn^{2+}) occurs primarily via LTCCs (Berkowitz et al., 2016). In a typical experiment, animals are dark adapted to maximally open LTCCs in, for example, the photoreceptor layer, followed by a systemic injection of a nontoxic dose of $MnCl_2$ (Berkowitz et al., 2016). The extent of retinal manganese uptake that occurs over the next four hours (while the animal is awake and freely moving) is then measured by MEMRI to assess the degree to which LTCCs were open (Berkowitz et al., 2016). Recently we implicated *in vivo* progressive, age-related increases in rod cell LTCC function in declining visual performance in 2-18 mo male Long-Evans rats (commonly considered an outbred rat strain) (Bissig et al., 2013). Indirect support for this calcium hypothesis of photoreceptor aging was also noted in 2-18 mo male C57BL/6 mice (an inbred mouse strain) which did not show escalating increases in rod LTCC function (MEMRI) nor visual performance declines (optokinetic tracking) (Berkowitz et al., 2014). It is unclear, however, if the different aging phenotypes between the outbred rat and inbred mouse are due to strain or genetic background. In this study, we examine the hypothesis that genetic diversity contributes to whether or not rod cell LTCC function escalates over time as measured by MEMRI. This hypothesis was tested by comparing young and old genetically heterogeneous UM-HET3 mice, generated from crossing two different F1 parents from The Jackson Laboratory: (BALB/cByJ × C57BL/6J)F1 mothers (CByB6F1/J; JAX Mice stock #100009) and (C3H/HeJ × DBA/2J)F1 fathers (C3D2F1/J; JAX Mice stock #100004).

Methods

All animals were treated in accordance with the National Institutes of Health Guide for the Care and Use of Laboratory Animals, the Association for Research in Vision and Ophthalmology Statement for the Use of Animals in Ophthalmic and Vision Research, and Institutional Animal and Care Use Committee authorization. Animals were housed and maintained in 12 hour:12 hour light-dark cycle laboratory lighting, unless otherwise noted.

Groups

4 mo and 18 mo genetically heterogeneous UM-HET3 mice were bred and reared at the University of Michigan before being shipped to Wayne State University for examination.

Optokinetic tracking (OKT)

Two visual performance metrics were evaluated in awake and freely moving mice: spatial frequency thresholds (SFT, "acuity", in cycles/degree, c/d) and contrast sensitivity (CS,

measured at the peak of the nominal curve (0.06 cycles/degree), inverse Michelson contrast (unitless)) using the optokinetic tracking reflex (OptoMotry, CerebralMechanics Inc., Alberta, Canada) (DOUGLAS et al., 2005). In brief, a vertical sine wave grating is projected as a virtual cylinder in three-dimensional coordinate space on computer monitors arranged in a quadrangle around a testing arena. Unrestrained mice (after an overnight dark adaptation) are placed on an elevated platform at the center of the arena. An experimenter used a video image of the arena from above to view the animal and follow the position of its head with the aid of a computer mouse and a crosshair superimposed on the mouse head. The X–Y positional coordinates of the crosshair are centered on the hub of the virtual cylinder, enabling its wall to be maintained at a constant “distance” from the animal's eyes, and thereby fixing the spatial frequency (SF) of the stimulus at the animal's viewing position. When the cylinder was rotated in the clockwise (CW) or counter clockwise (CCW) direction and the animal followed with head and neck movements that tracked the rotation, it was judged whether the animal's visual system could distinguish the grating. CW and CCW tracking provides a measure of left and right eye SFT and CS (DOUGLAS et al., 2005). One set of SFT and peak of CS measurements can reliably be obtained in 30 min.

Optical coherence tomography (OCT)

OCT (Envisu R2200 VHR SDOIS) was used to image retinal laminar spacing *in vivo* in a subset of mice from each age (n = 2). Mice were anesthetized with urethane (36% solution intraperitoneally; 0.083 ml/20 g animal weight, prepared fresh daily; Sigma-Aldrich, St. Louis, MO). OCT images were used to spatially calibrate the transretinal MRI profiles.

MRI

High resolution MRI of mouse retina is routinely performed in our laboratory (Berkowitz et al., 2016). All animals were maintained in darkness for at least 16 hrs before and during the dark-phase of the MRI examination. Mouse groups were either untreated, or treated with $MnCl_2$ (intraperitoneal injection, 66 mg $MnCl_2$•$4H_2O$ / kg)) either under dim red light (dark) or after 20 min of light exposure (Berkowitz et al., 2009;Berkowitz et al., 2014). After $MnCl_2$ injection, mice were maintained in the dark (or light) for another 3.5 to 4 hours. High resolution anatomical and apparent diffusion coefficient (ADC) data were acquired in the untreated mice on a 7 T system (Bruker ClinScan) using a receive-only surface coil (1.0 cm diameter) centered on the left eye; the presence of $MnCl_2$ does not alter ADC indices of light-evoked increases in water diffusion in the subretinal space (SRS) and in choroid thickness (Berkowitz et al., 2016;Berkowitz et al., 2015). The end of a fiber optic bundle was attached to a light source (Mark II Light Source; Prescott's Inc., Monument, CO) placed caudal to the eye, projecting at a white screen ~1 cm from eye, similar to that previously described (Bissig and Berkowitz, 2012). We exposed the eye to 0 (i.e., dark) or ~500 lux (confirmed outside the magnet using a Traceable Dual-Range Light Meter (Control Company, Friendswood, TX) placed against a 1 cm diameter aperture; measured this way, room lighting is ~300 lux). Aside from the fiber optic light source, all lights in the MRI room were turned off. In all groups, immediately before the MRI experiment, animals were anesthetized with urethane (36% solution intraperitoneally; 0.083 ml/20 g animal weight, prepared fresh daily; Sigma-Aldrich, St. Louis, MO) and treated topically with 1% atropine to ensure dilation of the iris during light exposure followed by 2% lidocaine to reduce eye

motion. Anatomical and ADC (parallel to the optic nerve) is the most sensitive direction for detecting changes in the extracellular space around the outer segments (Bissig and Berkowitz, 2012). ADC MRI data sets were collected, first in the dark and then again 15 min after turning on the light; since each ADC data set takes 10 min to collect, we refer to the mid-point in the ADC collection as 20 min of light exposure. Anatomical images were acquired using a spin-echo sequence (slice thickness 600 mm, TR 1000 ms, TE 11 ms, matrix size 192 × 320, field of view 8×8 mm^2, NA 2, axial resolution for central retina 25 mm). Images sensitized to water diffusion were collected [TR 1000 ms, slice thickness 600 mm, TE 33 ms, matrix size 174 × 288, field of view 8×8 mm^2, axial resolution for central retina 27.8 mm; b=0, 100, 250, 500, 600, 750, 990 s/mm^2 (collected in pseudo-random order, NA 1 per b value)], registered to the anatomical image, and analyzed (using in-house code) to generate ADC profiles from the central retina.

MEMRI data were acquired using several single spin-echo sequences (time to echo 13 ms, 7 × 7 mm^2, matrix size 160 × 320, slice thickness 600 μm). Images were acquired at different repetition times (TRs) in the following order (number per time between repetitions in parentheses): TR 0.15 seconds (6), 3.50 seconds (1), 1.00 seconds (2), 1.90 seconds (1), 0.35 seconds (4), 2.70 seconds (1), 0.25 seconds (5), and 0.50 seconds (3). To compensate for reduced signal-noise ratios at shorter TRs, progressively more images were collected as the TR decreased.

The present resolution in the central retina is sufficient for extracting meaningful layer-specific anatomical and functional data, as previously discussed (Berkowitz et al., 2015;Berkowitz et al., 2014). In all cases, animals were humanely euthanized as detailed in our DLAR-approved protocol.

Data analysis

In each animal, we confirmed ocular dilation based on the iris position on the anatomical MRI data; if eyelid position was closed to a degree likely to impede the light path, only the dark data from that animal were used (Bissig and Berkowitz, 2011). All images for each animal per lighting condition were registered (rigid body) to the anatomical image and ADCs in each pixel were calculated as previously described (Bissig and Berkowitz, 2011). In all cases, the same central retinal regions-of-interest (± 0.4 – 1 mm from the optic nerve head) were analyzed; thickness, ADC, and manganese uptake values from the superior and inferior retina were respectively averaged.

In each mouse, thicknesses (mm) from the anatomical and ADC images were objectively determined using the “half-height method” wherein a border is determined via a computer algorithm based on the crossing point at the midpoint between the local minimum and maximum, as detailed elsewhere (Bissig and Berkowitz, 2011;Cheng et al., 2006). The distance between two neighboring crossing-points thus represents an objectively defined thickness.

From the anatomical image, thickness measurements were normalized with 0% depth at the presumptive vitreoretinal border and 100% depth at the presumptive retina-choroid border.

Note that because of partial volume averaging there are slight contributions from non-retinal tissue anteriorly at the vitreoretinal border and posteriorly at the retina-choroid border.

Choroidal thickness in each mouse was determined as previously described (Berkowitz et al., 2015). We take advantage of the fact that ADC images show a suppressed signal from the vertical vessels between the horizontal segments of the choroid and the choroidal capillaries (i.e., the direction parallel to the optic nerve) and the vitreous (which has higher ADC than retina due to the lack of cellular barriers (Chen et al., 2008)). We then used the same computer algorithm as above to objectively determine the thickness from the portion of retina that was not suppressed in the averaged (to improve signal-to-noise) b100-b990 diffusion images. The thickness difference between that generated from the anatomical image (containing the choroid), and that generated from the ADC image (with a suppressed choroidal contribution), was considered an estimate of the choroid thickness for each mouse. In this manner, choroidal thicknesses were estimated for dark and light exposed conditions for each mouse; the accuracy of this choroidal thickness estimate has been confirmed in several models (Berkowitz et al., 2015).

As per our earlier studies, the ADC profiles in dark and light conditions in each mouse were spatially normalized to the anatomical thickness value in the dark (since our data indicated that the “extra” thickness in the light was primarily via expansion of the choroid in the light) (Berkowitz et al., 2015).

Evaluations of choroid and extracellular space around the outer segments were done objectively, based strictly on dark adapted anatomical thickness values (as described above), and thus data were not masked.

MEMRI data from the central retina (± 1 mm from the center of the optic nerve) were analyzed. Single images acquired with the same TR were first registered (rigid body) and then averaged. These averaged images were then registered across TRs. The same regions-of-interest as above were analyzed by calculating 1/T1 maps by first fitting to a three-parameter T1 equation (y=a + b*(exp(-c*TR)), where a, b, and c are fitted parameters) on a pixel-by-pixel basis using R (v.2.9.0, R Development Core Team [2009]). R: A language and environment for statistical computing. R Foundation for Statistical Computing, Vienna, Austria. ISBN 3–900051– 07–0) scripts developed in-house, and the minpack.lm package (v. 1.1.1, Timur V. Elzhov and Katharine M. Mullen minpack.lm: R interface to the Levenberg-Marquardt nonlinear least-squares algorithm found in MINPACK. R package version 1.1–1). The reciprocal (1/T1) values are proportional to manganese levels. Central intraretinal 1/T1 profiles were obtained as detailed elsewhere (Bissig and Berkowitz, 2011). Values from the superior and inferior retina were averaged. Note that only those animals that took up manganese above baseline (i.e., ~0.65 s^{-1}) were included in the final analysis.

Statistical analysis

Data are presented as mean ± standard error of the mean (SEM). All OKT and thicknesses in each group were evaluated for a normal distribution and each metric was compared between young and old mice using an unpaired t-test. In some animals, eyelids were not sufficiently open on MRI examination to prevent collection of light data from those mice. In young vs.

old mice, a generalized estimating equation (GEE) approach was used to compare only selected location ranges based on pre-specified knowledge of dark / light physiology (i.e., the SRS as measured by ADC MRI) and known location of rod cell LTCCs (i.e., in the outer nuclear layer) (Bissig and Berkowitz, 2012;Berkowitz et al., 2015;Berkowitz et al., 2016). The GEE method is a powerful two-tailed method that performs a general linear regression analysis using contiguous locations in each subject and accounts for the within-subject correlation between contiguous locations. Negative results are presented with 95% confidence intervals (95% CI).

Results

Aging UM-HET3 mice show visual performance declines without changes in LTCC function

Visual acuity and contrast sensitivity indices both decreased ($p < 0.05$) with age (Figure 1). However, no age-related differences (4 mo: 95% CI [1.28,1.36]; 18 mo: 95% CI [1.10,1.35]) were noted in the dark uptake of manganese suggesting no change with age in rod cell LTCC function and membrane polarization (Figure 2); dark is a condition that produces rod cell (and some inner retinal) membrane depolarization with opening of LTCCs.

Aging UM-HET3 mice do not show changes in light-evoked SRS and choroidal expansion, and in retinal anatomy

Light-evoked expansion at 80-100% depth, a measure of how well water produced by the rod cells during dark and light conditions is removed by the retinal pigment epithelium (Berkowitz et al., 2015), was greater than zero ($p < 0.05$) in both groups, and not different between young (27 ± 9%, mean ± SEM) and old (18 ± 6%) mice (4 mo: 95% CI [5.81 %, 48.8%]; 18 mo: 95% CI [1.88%, 34.65%]) (Figure 3). Also, light caused significant and similar degrees of expansion of the choroid in young (27 ± 8%) and older (36 ± 11%) mice (4 mo: 95% CI [6.62%, 46.6%]; 18 mo: 95% CI [6.09%, 66.32%]) (Figure 4). In addition, visual comparison of retinal laminar spacings between age groups (OCT) did not suggest an aging phenotype (Figure 4). Consistent with this, a quantitative analysis of whole retinal thicknesses found no difference between ages as measured by MRI (4 mo: 95% CI [198 mm, 225 mm]; 18 mo: 95% CI [194 mm, 214 mm]) (Figure 4).

Aging UM-HET3 mice show changes in choroidal thickness and chamber depth

Choroid thickness was reduced ($p < 0.05$) in older mice in dark and light conditions than in younger mice (Figure 4); these results are consistent with “healthy” age-related choroidal thinning in humans (Chhablani et al., 2014) and in pigeons (Fitzgerald et al., 2001). In addition, 18 mo mice had larger ($p < 0.05$) anterior chambers but smaller ($p < 0.05$) vitreous chambers than 4 mo mice (Figure 4).

Discussion

A major finding in this study is that aging of a genetically diverse mouse strain recapitulated a lack of changes in rod cell LTCC function previously observed in a commonly used inbred mouse strain (C57BL/6) but not the progressive increase in LTCC function seen in one stock of outbred rats (Bissig et al., 2013). A limitation of the present study is that only one

genetically heterogeneous mouse model is studied. However, UM-HET3 mice are constructed with unrelated parental strains in a four-way cross producing a population with wide genetic variation and greatly reduced homozygosity (Miller et al., 2002). This model thus seems reasonable for testing for a role of genetic heterogeneity *per se* as a major contributor to age-related progressive increase in rod cell LTCC function.

Somewhat unexpectedly, visual performance of UM-HET3 mice declined by 18 mo of age, unlike in C57BL/6 mice (Figure 1) (Berkowitz et al., 2014;Lehmann et al., 2012). This decline in vision occurred while rod cell LTCC function in the dark was maintained over time (Figure 2), while light-evoked expansion of the SRS and choroid were consistent with age, and without evidence for retinal thinning in older mice (Figures 3-4). It has been suggested that choroidal thinning is an independent factor underlying loss of vision, at least in pigeons (Fitzgerald et al., 2001). In this study, 18 mo UM-HET3 mice had thinner choroid than 4 mo mice. Since choroidal thickness is a major control-element of choroidal blood flow, and rod cell function appears normal, we speculate that perfusion of the posterior segment may be inadequate for the metabolic needs of the photoreceptors, a condition that could be linked with declines in visual performance. Intriguingly, unlike the UM-HET3 mice, C57BL/6 mice show neither choroidal thinning during aging nor vision loss (Berkowitz et al., 2014;Lehmann et al., 2012;Camelo et al., 2015). Together, these considerations raise the possibility that in mice choroidal thinning *per se* contributes to age-related declines in visual performance.

Intriguing, expansion of the anterior chamber (and decreased vitreous chamber depth) were noted between young and old UM-HET3 mice, and these are also common features of DBA2/J mice, a common murine glaucoma model with subnormal visual performance (Burroughs et al., 2011;Chou et al., 2011). However, this speculation requires additional testing.

In summary, unlike outbred Long-Evans rats, genetically heterogeneous mice show age-related vision deficits not related to increased rod cell LTCC channel function *in vivo*. The present data also raise the possibility that the age-related reduction in visual performance seen in the UM-HET3 mice was linked to changes in ocular anatomy often seen in age-related glaucoma, an observation requiring further investigation.

Acknowledgments

Supported by the National Eye Institute (EY021619 (BAB); EY026584 (BAB)), an unrestricted grant from Research to Prevent Blindness (Kresge Eye Institute), and National Institute of Aging (AG024824 (RM); AG022303 (RM)). Helpful discussion with Drs. Simon John and David Harrison are gratefully acknowledged.

References

Berkowitz BA, Grady EM, Khetarpal N, Patel A, Roberts R. Oxidative stress and light-evoked responses of the posterior segment in a mouse model of diabetic retinopathy. Invest Ophthalmol Vis Sci. 2015; 56:606–615. [PubMed: 25574049]

Berkowitz BA, Bissig D, Roberts R. MRI of rod cell compartment-specific function in disease and treatment in-vivo. Prog Retin Eye Res. 2016; 51:90–106. [PubMed: 26344734]

Berkowitz BA, Gradianu M, Bissig D, Kern TS, Roberts R. Retinal Ion Regulation in a Mouse Model of Diabetic Retinopathy: Natural History and the Effect of Cu/Zn Superoxide Dismutase

Overexpression. Investigative Ophthalmology Visual Science. 2009; 50:2351–2358. [PubMed: 19074809]

Berkowitz BA, Grady EM, Roberts R. Confirming a prediction of the calcium hypothesis of photoreceptor aging in mice. Neurobiol Aging. 2014; 35:1883–1891. [PubMed: 24680323]

Bissig D, Berkowitz BA. Light-dependent changes in outer retinal water diffusion in rats in vivo. Mol Vis. 2012; 18:2561. [PubMed: 23129976]

Bissig D, Berkowitz BA. Same-session functional assessment of rat retina and brain with manganese-enhanced MRI. NeuroImage. 2011; 58:749–760. [PubMed: 21749922]

Bissig D, Goebel D, Berkowitz BA. Diminished Vision in Healthy Aging Is Associated with Increased Retinal L-Type Voltage Gated Calcium Channel Ion Influx. PLoS ONE. 2013; 8:e56340. [PubMed: 23457553]

Burroughs SL, Kaja S, Koulen P. Quantification of Deficits in Spatial Visual Function of Mouse Models for Glaucoma. Invest Ophthalmol Vis Sci. 2011; 52:3654–3659. [PubMed: 21330670]

Camelo S, Calippe B, Lavalette S, Dominguez E, Hur J, Devevre E, Guillonneau X, Raoul W, Sennlaub F. Thinning of the RPE and choroid associated with T lymphocyte recruitment in aged and light-challenged mice. Mol Vis. 2015; 21:1051–1059. [PubMed: 26392743]

Chen J, Wang Q, Zhang H, Yang X, Wang J, Berkowitz BA, Wickline SA, Song SK. In vivo quantification of T1, T2, and apparent diffusion coefficient in the mouse retina at 11.74T. Magn Reson Med. 2008; 59:731–738. [PubMed: 18383302]

Cheng H, Nair G, Walker TA, Kim MK, Pardue MT, Thule PM, Olson DE, Duong TQ. Structural and functional MRI reveals multiple retinal layers. Proc Natl Acad Sci U S A. 2006; 103:17525–17530. [PubMed: 17088544]

Chhablani J, Wong IY, Kozak I. Choroidal imaging: A review. Saudi J Ophthalmol. 2014; 28:123–128. [PubMed: 24843305]

Chou TH, Kocaoglu OP, Borja D, Ruggeri M, Uhlhorn SR, Manns F, Porciatti V. Postnatal Elongation of Eye Size in DBA/2J Mice Compared with C57BL/6J Mice: In Vivo Analysis with Whole-Eye OCT. Invest Ophthalmol Vis Sci. 2011; 52:3604–3612. [PubMed: 21372015]

Douglas RM, Alam NM, Silver BD, McGill TJ, Tschetter WW, Prusky GT. Independent visual threshold measurements in the two eyes of freely moving rats and mice using a virtual-reality optokinetic system. Vis Neuro. 2005; 22:677–684.

Fitzgerald ME, Tolley E, Frase S, Zagvazdin Y, Miller RF, Hodos W, Reiner A. Functional and morphological assessment of age-related changes in the choroid and outer retina in pigeons. Vis Neuro. 2001; 18:299–317.

Lehmann K, Schmidt KF, Löwel S. Vision and visual plasticity in ageing mice. Restorative Neurology and Neuroscience. 2012; 30:161–178. [PubMed: 22348872]

Miller RA, Chrisp C, Jackson AU, Galecki AT, Burke DT. Coordinated Genetic Control of Neoplastic and Nonneoplastic Diseases in Mice. The Journals of Gerontology Series A: Biological Sciences and Medical Sciences. 2002; 57:B3–B8.

Swindell W, Ensrud K, Cawthon P, Cauley J, Cummings S, Miller R, Study Of Osteoporotic Fractures Research Group. Indicators of “Healthy Aging” in older women (65-69 years of age). A data-mining approach based on prediction of long-term survival. BMC Geriatrics. 2010; 10:55. [PubMed: 20716351]

Highlights

- Vision of aging UM-HET3 mice declined without rod calcium channel dysfunction.
- Impaired vision correlated with ocular anatomical changes but not retinal thinning.
- Genetic diversity alone does not appear to contribute to visual declines over time.

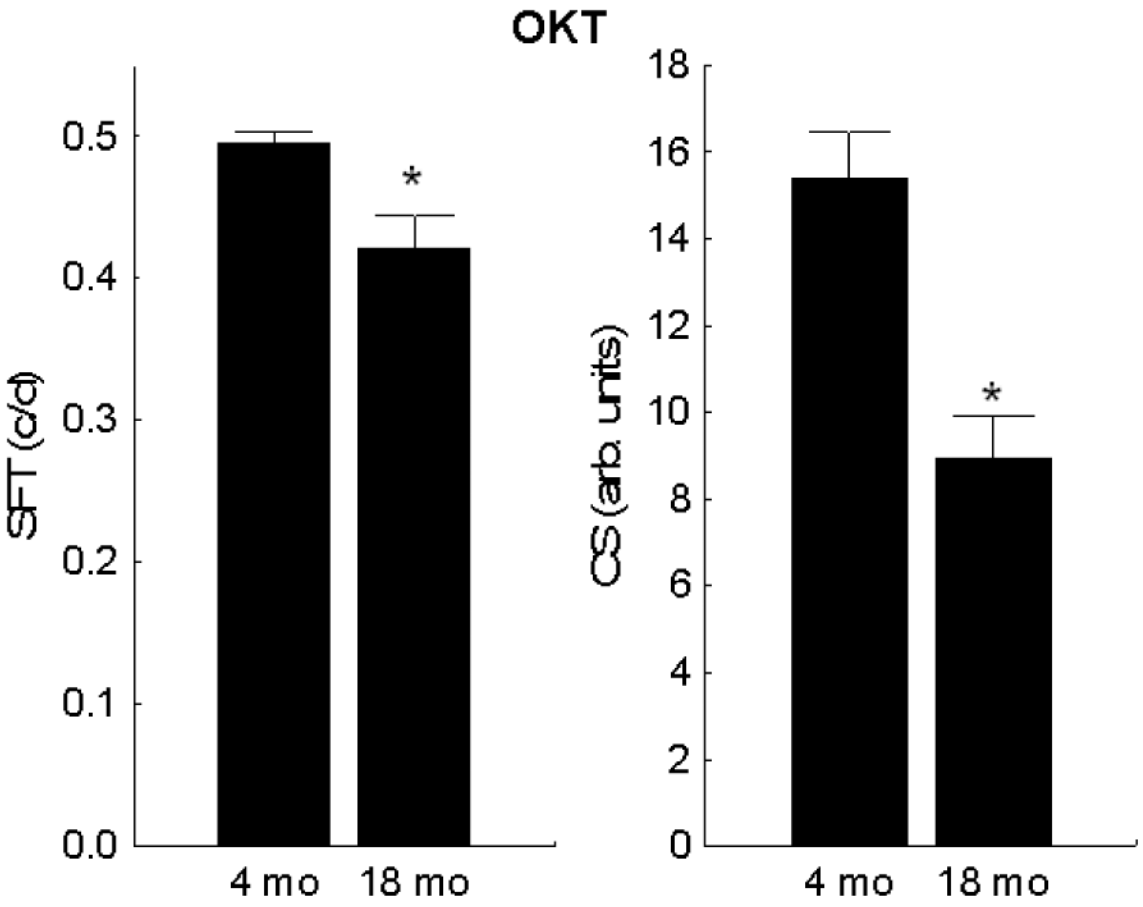

Figure 1. Visual performance of UM-HET3 mice declines with age

Visual indices evaluated for young (n = 8) and old (n = 8) mice were spatial frequency threshold (left panel) and presumptive peak of the contrast sensitivity curve (right panel). Significant differences ($p < 0.05$) from 4 mo (*) are noted. Error bars represent SEM.

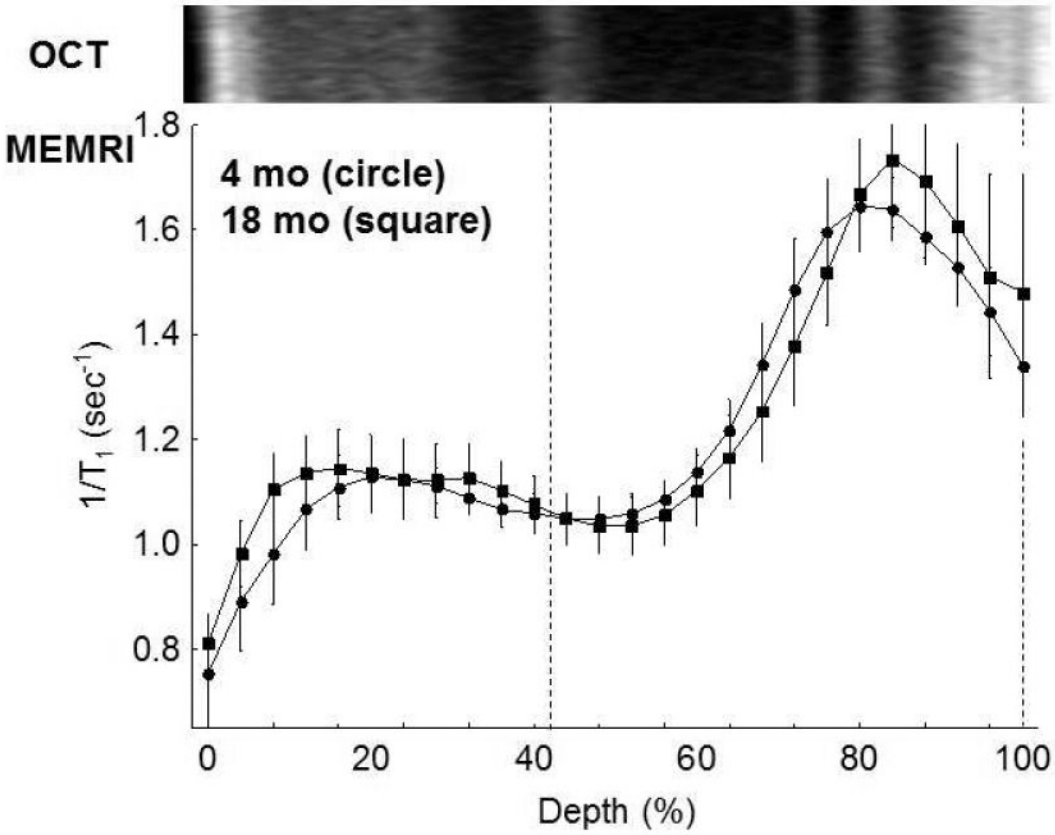

Figure 2. Functional rod cell LTCC topography as measured by MEMRI does not increase with age

Summary of central retinal MEMRI as a function of retinal depth in dark adapted 4 mo (n = 5) and 18 mo UM-HET3 (n = 5) mice. Approximate location of two anatomical landmarks are indicated by dotted lines (i.e., anterior aspect of the outer plexiform layer (left) and retina/choroid border (right)). Profiles are spatially normalized to dark adapted retinal thickness (0% = vitreous/retina border, 100% = retina / choroid border) and spatially calibrated against a representative optical coherence tomography image from a 4 mo mouse; as shown in Figure 4, OCT and retinal thickness does not change with age (see text). Error bars, SEM.

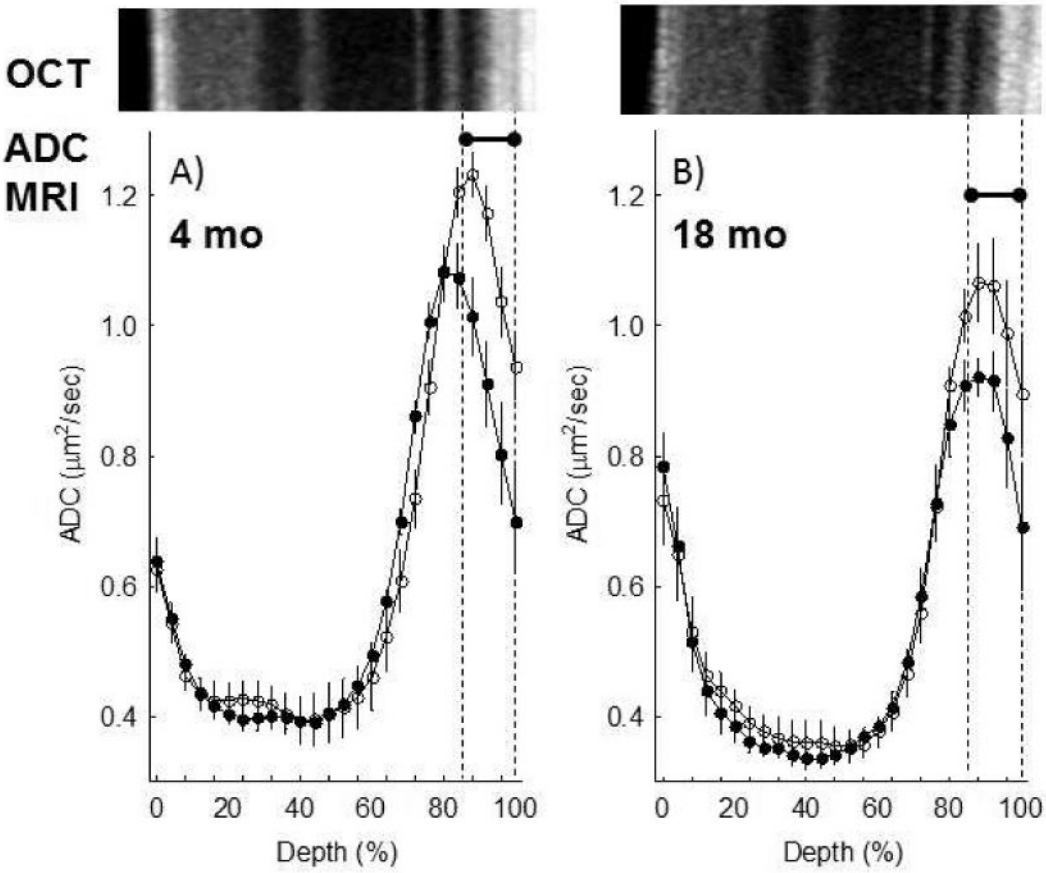

Figure 3. Light-evoked increase in SRS as measured by diffusion weighted MRI does not change with age

Summary of central retinal ADC as a function of retinal depth during dark (*closed symbols*) and at 20 minutes of ~500 lux light (*open symbols*) in A) 4 mo (n = 7) and B) 18 mo UM-HET3 (n = 5) mice. Data are presented using the conventions in Figure 2. *Retinal depth range with significant difference ($P < 0.05$).

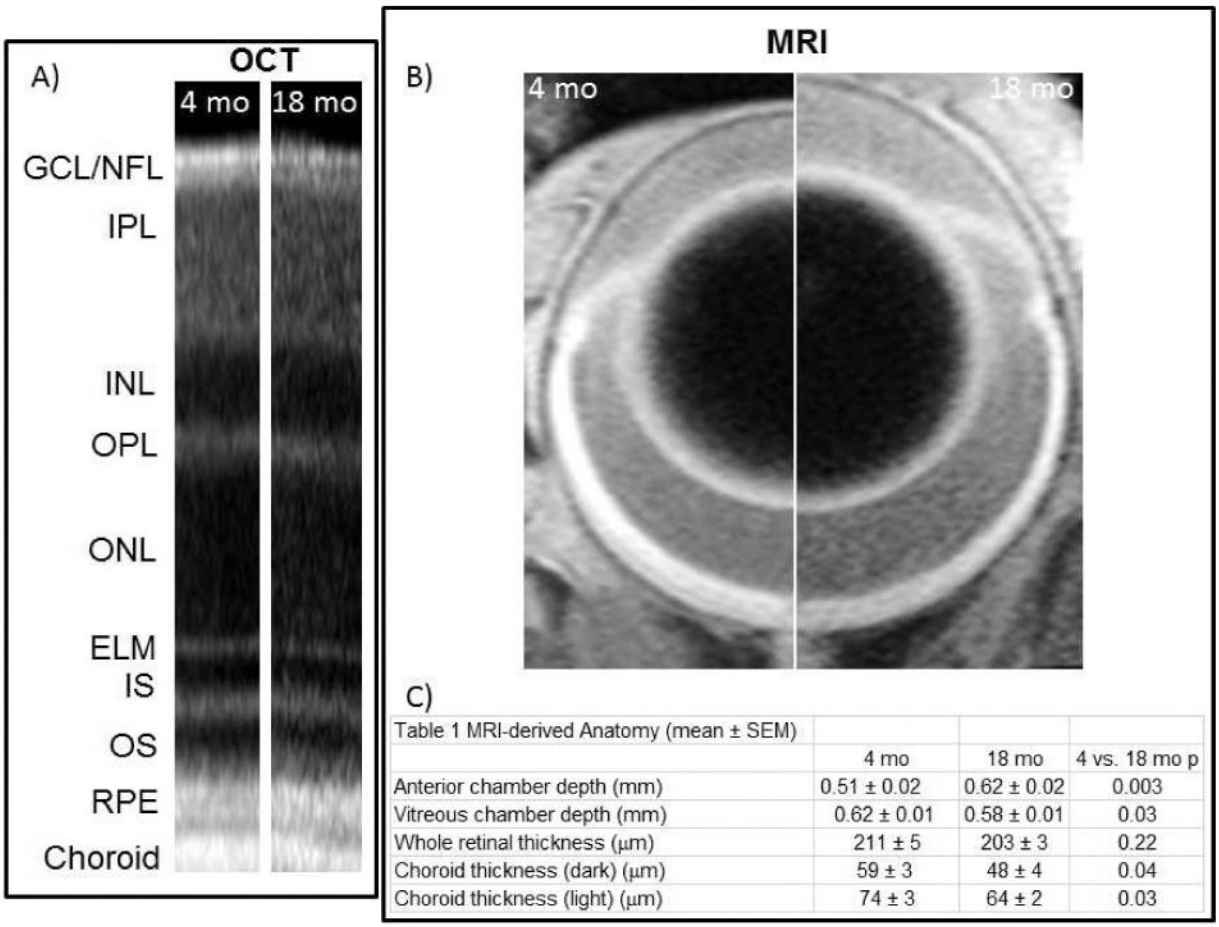

C)

Table 1 MRI-derived Anatomy (mean ± SEM)			
	4 mo	18 mo	4 vs. 18 mo p
Anterior chamber depth (mm)	0.51 ± 0.02	0.62 ± 0.02	0.003
Vitreous chamber depth (mm)	0.62 ± 0.01	0.58 ± 0.01	0.03
Whole retinal thickness (μm)	211 ± 5	203 ± 3	0.22
Choroid thickness (dark) (μm)	59 ± 3	48 ± 4	0.04
Choroid thickness (light) (μm)	74 ± 3	64 ± 2	0.03

Figure 4. Age alters ocular anatomy of UM-HET3 mice

A) Representative OCT data from 4 and 18 mo UM-HET3 mice (RGC/NFL: retinal ganglion cell layer / nerve fiber layer; IPL: inner plexiform layer; INL: inner nuclear layer; OPL: outer plexiform layer; ONL: outer nuclear layer; ELM: external limiting membrane; IS: inner segments of rod cells (ellipsoid region); OS: outer segments of rod cells; RPE: retinal pigment epithelium). B) Representative MRI images obtained in 4 mo (left half) and 18 mo (right half) mice. Images are displayed at the same magnification. C) Summary of anatomical measurements from 4 mo (n = 7) and 18 mo UM-HET3 (n = 5) mice.